Physics of the Solid State, Vol. 46, No. 11, 2004, pp. 2067–2072. Translated from Fizika Tverdogo Tela, Vol. 46, No. 11, 2004, pp. 2000–2005.

MAGNETISM AND FERROELECTRICITY

Spin-Dependent Transport in α-MnS Single Crystals

S. S. Aplesnin, L. I. Ryabinkina, G. M. Abramova, O. B. Romanova, N. I. Kiselev, and A. F. Bovina

Kirensky Institute of Physics, Siberian Division, Russian Academy of Sciences, Akademgorodok, Krasnoyarsk, 660036 Russia

e-mail: lir@iph.krasn.ru

Received January 29, 2004

Abstract—The electrical resistivity of single crystal α-MnS in crystallographic directions [111] and [100] was found to be anisotropic in the temperature interval 77–300 K. The change in activation energy below the Néel temperature was determined. Magnetoresistance was revealed, and reversal of its sign in the (111) plane above the Néel point was found. The experimental data are analyzed in terms of the *s–d* model, with the manganese ion holes interacting with localized spins assumed to be free carriers. © *2004 MAIK "Nauka/Interperiodica".*

1. INTRODUCTION

A new direction in science, spintronics, has recently been undergoing explosive development [1]. Spintronics draws on the dependence of conductivity on magnetic structure, which changes when acted upon by an external magnetic field. The use of nanotechnology in electronic devices places constraints on the area of application of *p–n* junction–based semiconductors and calls for using alternative materials that have strongly interrelated magnetic and electronic properties. Manganites figure among such materials. They have the remarkable feature of exhibiting giant magnetoresistance at room temperature, with the resistivity in an external magnetic field varying over more than an order of magnitude. The effect of magnetic order on transport properties also becomes manifest in the sulfide systems $Me_xMn_{1-x}S$ (*Me* = Cr, Fe), which are prepared on the basis of the monosulfide α-MnS and exhibit colossal magnetoresistance [2]. Off-stoichiometry in the α-MnS magnetic semiconductor also brings about a change in the magnetic structure and a substantial variation in resistivity [3].

We report on a study of the relation between the magnetic, electronic, and elastic subsystems in the α-MnS magnetic semiconductor. The manganese monosulfide α-MnS is an antiferromagnet with an fcc lattice. Its magnetic structure combines ferromagnetic ordering of the magnetic moments of manganese ions in (111)-type planes and antiferromagnetic interplane ordering with a Néel temperature $T_N \approx 150$ K [3, 4]. Antiferromagnetic ordering is also observed to set in along the cube edges. It thus appeared reasonable to investigate the effect of magnetic ordering on the transport properties of an α-MnS single crystal in (111)- and (100)-type planes. The experimental data obtained are analyzed in terms of the *s–d* model in the strong-coupling limit, where the conduction band width $W \ll I$ (I is the *s–d* exchange integral), which is valid for magnetic semiconductors with a narrow conduction band.

2. EXPERIMENTAL TECHNIQUES AND EXPERIMENTAL RESULTS

An α-MnS single crystal was grown by saturating liquid manganese with sulfur at $T \sim 1245$°C. X-ray structural analysis was performed on a DRON-2.0 diffractometer with CuK_α radiation in the temperature interval 77–300 K. X-ray fluorescence analysis was carried out on a SPARK-1 x-ray spectrometer. The electrical resistivity in the (100) and (111) crystallographic planes was measured in zero magnetic field and in transverse magnetic fields of up to 15 kOe in the temperature interval 77–300 K. The magnetoresistance was calculated using the relation $\delta_H^{ex} = \dfrac{\rho(H) - \rho(H=0)}{\rho(H)} \times 100\%$.

The x-ray diffraction measurements showed the α-MnS single crystal to have a NaCl-type fcc lattice with the parameter $a = 5.222 \pm 0.001$ Å, which agrees well with the data obtained on α-MnS single crystals grown using chemical transport reactions [5]. The x-ray fluorescence analysis suggests the absence of impurities in the α-MnS single crystal. Figure 1 shows the temperature dependence of the lattice parameter, which decreases nonlinearly with decreasing temperature. The variation in $a(T)$ is maximum in the region (166–125) ± 5 K, where the NaCl-type fcc lattice was shown in [5] to undergo a rhombohedral distortion.

Figure 2 plots the temperature dependence of electrical resistivity in the (111) and (100) crystallographic planes obtained in zero magnetic field in the temperature interval 77–300 K. When measured at ~300 K, the electrical resistivity of the crystal is 3.17×10^5 Ω cm in the (100) plane and 5.98×10^5 Ω cm in the (111) plane.

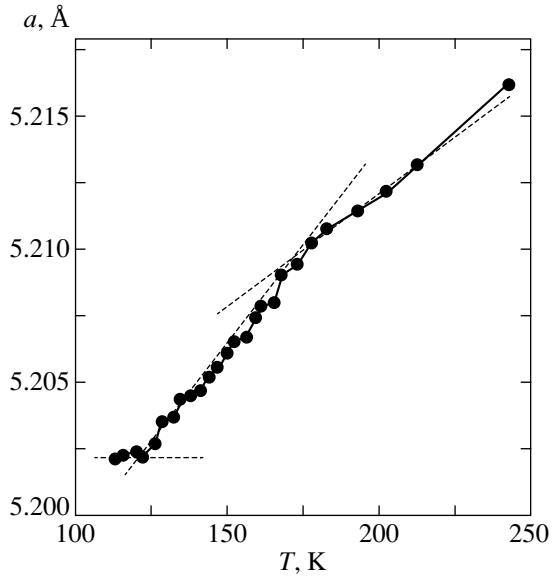

Fig. 1. Temperature dependence of the lattice parameter of a manganese monosulfide single crystal.

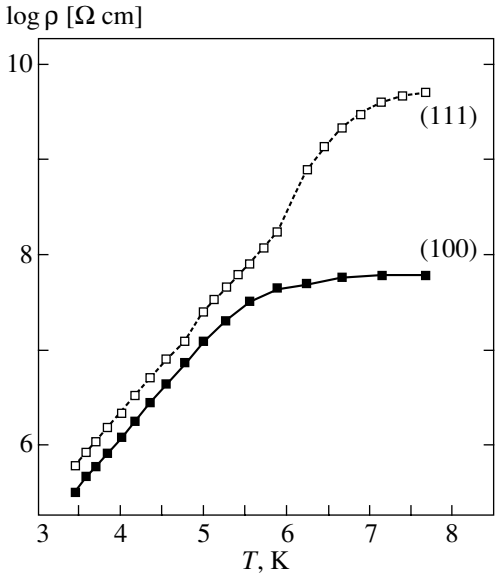

Fig. 2. Temperature dependence of the electrical resistivity of α-MnS in the (111) and (100) planes.

For temperatures $T \sim 170$–300 K, the conductivity can be fitted by a relation typical of semiconductors, $\sigma \sim \exp(-E_a/k_BT)$, with activation energy $E_a \sim 0.2$ eV. For $T < 160$ K, the electrical resistivity in the (111) plane increases, which is accompanied by the conductivity activation energy decreasing down to $E_a \sim 0.04$ eV below T_N. An analysis of the behavior of electrical resistivity in the (100) plane measured in zero magnetic field shows $\rho(T)$ not to be activated thermally for $T < T_N$.

The magnetoresistance of α-MnS was studied by measuring the electrical resistivity in the (111) and (100) planes in the temperature interval 77–300 K and magnetic fields of up to 15 kOe. Figures 3a and 3b plot temperature dependences of the magnetoresistance measured in the (111) and (100) planes of α-MnS, respectively, in a field of 10 kOe at temperatures of 100–300 K. It was established that the magnetoelectric properties, as well as the electrical properties, depend on crystallographic orientation. The negative magnetoresistance reaches –12% at 10 kOe and becomes most pronounced in the (111) plane at temperatures $T \sim 230$ K. The maximum positive magnetoresistance in the (100) plane in the same field is +11% in the region of the magnetic transition point. As the magnetic field increases, the minimum negative magnetoresistance in the (111) plane does not change in magnitude but shifts to low temperatures; indeed, in a field of 15 kOe, the minimum is seen at $T \sim 170$ K. The observed variation in magnetoresistance is reversible.

3. MODEL AND METHOD OF CALCULATION

Hall measurements performed for $T < 450$ K suggest [4] that the conduction in α-MnS is due to holes in the 3*d* levels of the manganese ion. This conclusion is also supported by calculations made using the electronic density functional method [6]. For instance, the hole concentration in the t_{2g} and e_g shells is 0.11 and 0.29 per Mn^{2+} ion, respectively. The rhombohedral distortion of the fcc lattice occurring near the Néel temperature brings about a weak overlap of the t_{2g} shells of neighboring manganese ions and the formation of a narrow energy band. For $T > T_N$, the low mobility of the holes caused by their being trapped by dynamic rhombohedral distortions supports the validity of assuming a narrow Mn^{2+} band.

Since the hole concentration is much less than unity, we neglect the Coulomb interaction of holes at a site and consider a gas of holes interacting with the localized manganese ion spins in the *s*–*d* model, an instructive approach that simplifies a qualitative understanding of the experimental results obtained.

We treat the magnetic and electronic properties in the adiabatic approximation. We define the magnetic structure in the Heisenberg model with antiferromagnetic interaction between the nearest (J_s) and next-to-nearest (K) neighbors mediated by sulfur ions:

$$H = -\sum_{i,j} J_{i,js}\mathbf{S}_i\mathbf{S}_j - \sum_{i,j} K_{i,j}\mathbf{S}_i\mathbf{S}_j - \sum_i H_iS_i, \qquad (1)$$

where H_i is an external magnetic field.

The electronic properties will be considered in terms of the *s*–*d* model with an Ising-type Hamiltonian [7]:

$$H = H_{\text{kin}} + H_{\text{int}}, \quad H_{\text{kin}} = \sum_{ij\sigma} t_{ij} a^{+}_{i\sigma} a_{i\sigma},$$
$$H_{\text{int}} \longrightarrow -\frac{1}{2} J_H \sum_I S^z_i (a^{+}_{i\uparrow} a_{i\uparrow} - a^{+}_{i\downarrow} a_{i\downarrow}), \tag{2}$$

where S^z_i is the operator of the z component of the localized spin at site i; J_H is the Hund exchange parameter; t_{ij} is the matrix element of hole transfer over the lattice, which depends on the mutual orientation of spins at sites i and j involved in the hole transfer; and $a^{+}_{i\sigma}$ ($a_{i\sigma}$) is the Fermi operator of creation (annihilation) of a hole with spin σ at site i. In second order of perturbation theory in parameter W/J_H (W is the band width), one can switch from the original Hamiltonian $H = H_{\text{kin}} + H_{\text{int}}$ with simplified interaction (2) to the effective Hamiltonian

$$H = -t \sum c^{+}_{i\sigma} c_{i\sigma} - \sum J^h_{ij} n_{i\sigma} n_{i\sigma}. \tag{3}$$

Here, J^h is the indirect interaction between the nearest neighbor sites ($J^h \sim t^2/J_H$), $n_{i\sigma} = c^{+}_{i\sigma} c_{i\sigma}$, and $c_{i\sigma}(c^{+}_{i\sigma})$ is the Fermi-like annihilation (creation) operator for a complex consisting of a localized spin at site i and a hole with a parallel spin,

$$c_{i\sigma} = \frac{1}{2}(1 + \sigma S^z_i) a_{i\sigma}. \tag{4}$$

The states of sites at which the spins in the complexes described by operators $(1/2)(1 - \sigma S^z_i)a_{i\sigma}$ are antiparallel are disregarded [8]. In the limit as $z \longrightarrow \infty$, the Hartree–Fock approximation of intersite interaction becomes exact; therefore, the exchange term in Eq. (3) can be linearized and the Hamiltonian can be recast in the form

$$H = \sum \varepsilon_\sigma c^{+}_{i\sigma} c_{i\sigma} - t \sum c^{+}_{i\sigma} c_{i\sigma}, \tag{5}$$

where $\varepsilon_\sigma = -\mu - \sum_j J^h_{ij} \langle n_{j\sigma} \rangle$ and μ is the chemical potential.

Using a special diagrammatic technique, Izyumov and Letfulov [8] obtained the following coupled equations to determine the magnetizations m^s and m^d of itinerant and localized spins, respectively, and the chemical potential μ:

$$m^d = \tanh \frac{1}{2} \lambda,$$

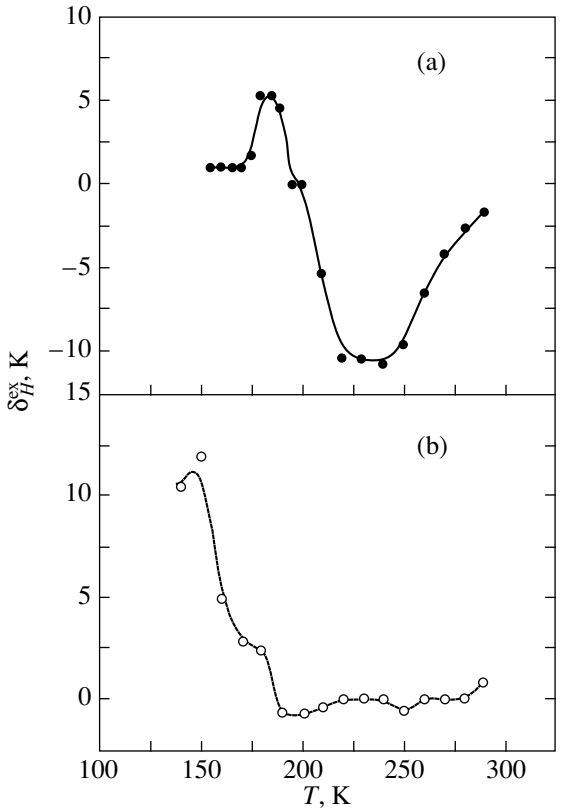

Fig. 3. Temperature dependence of the magnetoresistance $\delta^{ex}_H = [(\rho(H) - \rho(H=0))/\rho(H)] \times 100\%$ of α-MnS in a magnetic field H = 10 kOe in (a) the (111) and (b) (100) planes.

$$\lambda = \frac{1}{\pi} \int_0^\pi dt \ln \frac{1 + \exp\beta(\mu_r - \nu - a_\uparrow \cos t)}{1 + \exp\beta(\mu_r + \nu - a_\downarrow \cos t)},$$
$$m^s = n m^d + [1 - (m^d)^2] \sum_\sigma \sigma \frac{1}{\pi} \int_0^\pi dt \sin^2 t \, f(a_\sigma \cos t + \sigma\nu), \tag{6}$$
$$n = \sum_\sigma (1 + \sigma m^d) \frac{1}{\pi} \int_0^\pi dt \sin^2 t f(a_\sigma \cos t + \sigma\nu).$$

Here, $\mu_r = \mu + I_h n/2$, $n = \langle n_{i\uparrow} \rangle + \langle n_{i\downarrow} \rangle$, $\nu = (1/2) I_h m^s$, $I_h = zJ^h$, $a^2_\sigma = (1/8)W^2(1 + \sigma m^d)$, $\beta = 1/T$, and $f(x)$ is the Fermi distribution function.

We will use these equations to determine the chemical potential, bandwidth, and hole concentration as functions of localized spin magnetization in the (111) plane. For temperatures above the Néel point, we will include the interaction of holes with the short-range localized spin order, i.e., the parameter $(m^d)^2 = (4/L) \sum_r^{L/4} \langle S^z(0) S^z(r) \rangle$.

The magnetic structure and thermodynamic characteristics for localized spins were calculated using the

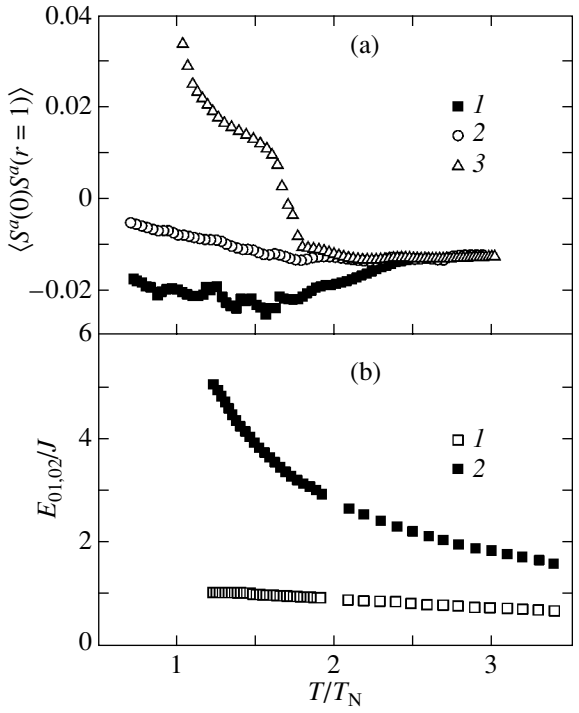

Fig. 4. (a) Spin–spin correlation function $\langle S^\alpha(0)S^\alpha(r = 1)\rangle$ for nearest neighbors along the [011] direction calculated for (*1*) $\alpha = x$, (*2*) y, and (*3*) z. (b) Local spin interaction energies (*1*) $E_{01}/J = \sum_{\alpha = x, y, z}\sum_{h = 1}^{12} S_0^\alpha S_h^\alpha$ and (*2*) $E_{02}/J = (K/J)\sum_{\alpha = x, y, z}\sum_{h = 1}^{6} S_0^\alpha S_h^\alpha$ in the first and second coordination shells, respectively, plotted vs. normalized temperature T/T_N.

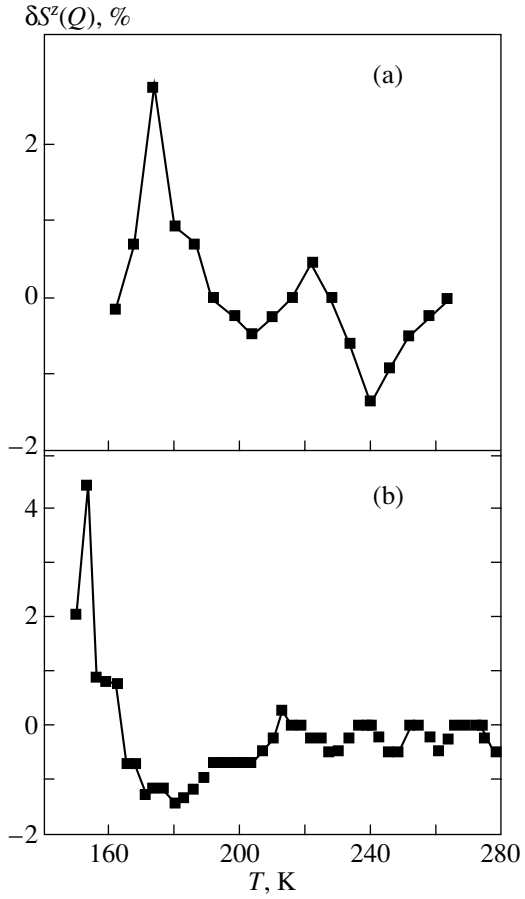

Fig. 5. Relative variation of the magnetic structural factor in the (111) plane, $\delta S^z = [(S^z(Q, H) - S^z(Q, H = 0)/S^z(Q, H)] \times 100\%$, in a magnetic field (a) $H = 8$ and (b) 16 kOe plotted vs. temperature for wave vector $Q \leq 0$.

Monte Carlo technique (MC) in classical Heisenberg model (1) with the exchange energy ratio $K/J = 1.85$ determined earlier in [9]. The procedure used periodic boundary conditions imposed on a $20 \times 20 \times 20$ grid with 30000 MC steps per spin.

4. RESULTS AND DISCUSSION

The fcc lattice of α-MnS contains the maximum number of frustrated spin exchange bonds: the numbers of nearest neighbors with parallel spins and with antiparallel spins are equal, and the local energy for Ising spins is $E_{01}/J = \sum_{h = 1}^{12} S_0 S_h = 0$.

In the classical Heisenberg model, frustration accounts for a noncollinear spin arrangement. For $T \ll T_N$, the contribution from the transverse spin components to $E_{0.1}/J$ is ≈2, which is approximately 3% of the maximum contribution, and their contribution to the exchange interaction energy in the second coordination shell $E_{02}/J = (K/J)\sum_{h = 1}^{h = 6} S_0 S_h$ is about 12%. For certain directions, the sign of the spin–spin correlation functions of transverse spin components does not coincide with the sign of the spin–spin correlation functions of longitudinal spin components calculated for the cube face diagonals. Figure 4a presents graphs of typical temperature dependences of the nearest neighbor correlation functions in the [011] direction. The transverse spin components in the (111) plane are possibly disordered.

As one crosses the Néel temperature, the short-range magnetic spin order for $T > T_N$ corresponds to the long-range magnetic order. The correlation length of the spin–spin correlation functions in the paramagnetic phase decreases following a power law. The exchange interaction energy in the second coordination shell E_{02} falls off rapidly, whereas the energy E_{01} is practically independent of temperature (Fig. 4b). In the vicinity of the temperature $T^* \approx 1.6T_N$, the type of short-range magnetic order changes. Indeed, as seen from Fig. 4a, the nearest neighbor spin–spin correlation function $\langle S^z(0)S^z(r = 1)\rangle$ becomes negative in the (111) plane. An external magnetic field applied perpendicular to the (111) plane reduces the correlation length and decreases the temperature at which the type of short-

range order changes. The magnetic structural factor in the (111) plane also decreases in magnitude. The corresponding relative change $\delta S^z(Q) = [S^z(Q, H) - S^z(Q, H = 0)]/S^z(Q, H)$ with temperature (Q is the wave vector) is displayed graphically in Fig. 5. Near the Néel temperature, the magnetic field suppresses a noncollinear spin arrangement and thereby increases the correlation functions of longitudinal components. This case is a typical for frustrated systems, where an external magnetic field brings about destruction of a noncollinear structure.

Using the known hole concentration $n \approx 0.1$ [4] at $T = 435$ K, we calculated the indirect interaction parameter $I_h = 9.3$ meV and the Hund exchange integral $J_H \approx 4$ eV. The calculated parameters correlate well with $J_H \approx 3.8$ eV and $W \approx 1$ eV from [3]. The interaction of the hole spins with localized spins exhibiting short-range magnetic order in the (111) plane splits the upper and lower hole band edges. This effect manifests itself particularly clearly below the Néel temperature, as seen from Fig. 6. Because of the strong s–d coupling, a localized spin is bonded in a complex with a band hole, which results in efficient attraction of the hole to the site and in a gap opening at the Fermi level below T_N in the (111) plane. The temperature dependence of the gap is shown in Fig. 7.

Manganese ions arranged along the cube edges are coupled by indirect antiferromagnetic exchange interaction mediated by sulfur ions, and hole hopping without spin flip is possible by the double exchange mechanism. The double-exchange model allows the formation of a weak ferromagnetic moment ($m_0 \ll m_d$) [7] and nonactivated conductivity in the [100] direction. In a magnetic field, the magnetic structural factor changes (Fig. 5) and the position of the chemical potential changes relative to the Fermi level (inset in Fig. 7). As a result, the electrical resistivity in the (111) plane undergoes a change, because $\ln\rho \sim (E_F - \mu)/k_B T$. The calculated temperature ranges corresponding to negative and positive changes in the quantity $\{(E_F - \mu)_H - (E_F - \mu)_{H=0}\}$ are in good agreement with those over which positive and negative values of magnetoresistance are observed.

The temperature derivative of the chemical potential $d\mu/dT$ has a minimum tending to zero at the Néel temperature. The temperature behavior of $\mu(T)$ is shown in Fig. 6. According to [8], the thermopower is proportional to $d\mu/dT$. The experimentally observed growth of thermopower for $T > T_N$ [4] agrees qualitatively with our results. The compressibility coefficient κ is defined as the second derivative with respect to energy and is given by

$$\frac{1}{\kappa} = \frac{\partial^2 E}{\partial n^2} = \left(\frac{\partial n}{\partial \mu}\right)^{-1}. \qquad (7)$$

The compressibility coefficient reverses sign from negative to positive near the Néel temperature at $T =$ 162 K. The dependence of the hole concentration on the chemical potential is presented graphically in Fig. 8. The negative compressibility coefficient in the temperature interval $125 < T < 162$ K should be attributed to

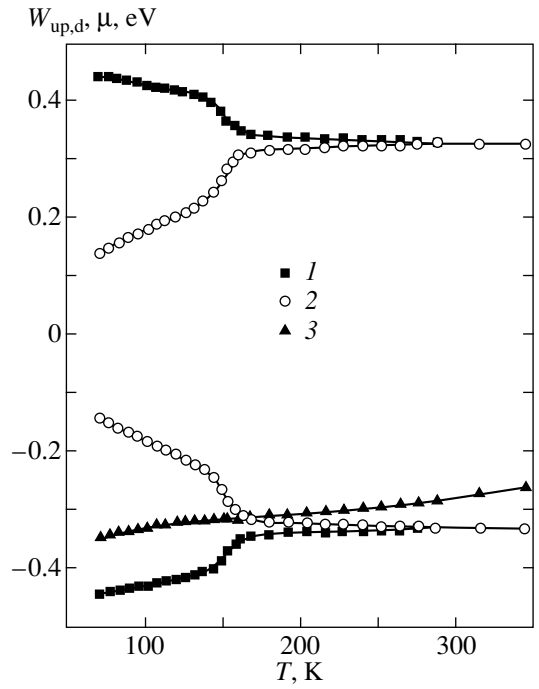

Fig. 6. Temperature dependences (*1*, *2*) of the upper and lower edges of the (*1*) spin-up and (*2*) spin-down subbands and (*3*) of the chemical potential.

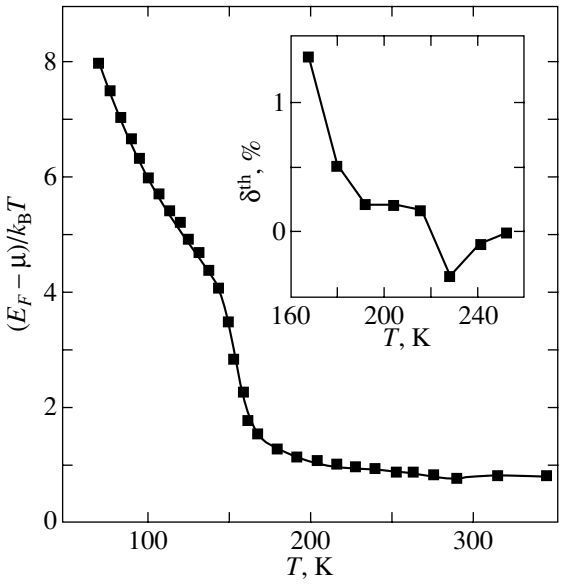

Fig. 7. Temperature dependence of the difference between the Fermi energy and the chemical potential. Inset: calculated shift in chemical potential relative to the Fermi level $\delta^{th} = [\{(E_F - \mu)_H - (E_F - \mu)_{H=0}\}/(E_F - \mu)_H] \times 100\%$ in a magnetic field $H = 8$ kOe plotted vs. temperature.

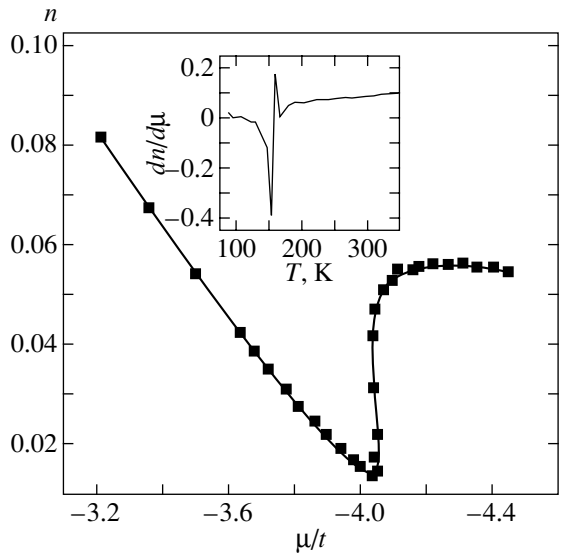

Fig. 8. Dependence of the hole concentration on the chemical potential normalized against the hopping integral t. Inset: temperature dependence of compressibility coefficient $dn/d\mu$ for a hole gas.

the sharp increase in the hole concentration. This brings about a decrease in Coulomb interaction between the ions and, possibly, a change in the elastic modulus of the α-MnS crystal. Furthermore, additional ferromagnetic exchange interaction mediated by delocalized holes appears between the localized spins in the (111) plane, which gives rise to a rhombohedral distortion of the fcc lattice observed to occur in α-MnS [4]. The distortion angle is directly proportional to the exchange interaction J^h and inversely proportional to the elastic modulus of the crystal [10]. Exchange-induced striction compresses the lattice. The calculated temperature interval over which the compressibility coefficient is negative correlates well with the temperature region in which the lattice constant is observed to undergo the maximum change (Fig. 1).

5. CONCLUSIONS

The pronounced increase in the resistivity anisotropy observed in an α-MnS single crystal below the Néel temperature is induced by the hole spins interacting with ferromagnetically ordered localized spins in the (111) plane and by gap formation at the Fermi level, which correlates qualitatively with the activated character of the conductivity in the (111) plane. The sign reversal of magnetoresistance in α-MnS in the (111) plane is initiated by a change in magnetic order for $T > T_N$; indeed, the disappearance of long-range magnetic order gives rise to positive magnetoresistance at $T \sim 160$ K and the destruction of short-range magnetic order causes negative magnetoresistance at $T \sim 230$ K. The additional exchange interaction created by the holes leads to compression and rhombohedral distortion of the lattice in the (111) plane below the Néel temperature.

ACKNOWLEDGMENTS

The authors are indebted to G.A. Petrakovskiĭ for helpful discussions and to G.V. Bondarenko for performing the x-ray fluorescence analysis.

This study was supported by the program of the Presidium of the Russian Academy of Sciences (project "New Materials for Technology") and, in part, by the Russian and Belarussian Foundations for Basic Research (project no. 04-02-81018 Bel2004_a).

REFERENCES

1. A. V. Vedyaev, Usp. Fiz. Nauk **172** (12), 1458 (2002) [Phys. Usp. **45**, 1296 (2002)].
2. G. A. Petrakovskiĭ, L. I. Ryabinkina, G. M. Abramova, N. I. Kiselev, A. D. Velikanov, and A. F. Bovina, Pis'ma Zh. Éksp. Teor. Fiz. **69** (12), 895 (1999) [JETP Lett. **69**, 949 (1999)]; G. A. Petrakovskiĭ, L. I. Ryabinkina, G. M. Abramova, A. D. Balaev, D. A. Balaev, and A. F. Bovina, Pis'ma Zh. Éksp. Teor. Fiz. **72** (2), 99 (2000) [JETP Lett. **72**, 70 (2000)].
3. G. V. Loseva, S. G. Ovchinnikov, and L. I. Ryabinkina, Fiz. Tverd. Tela (Leningrad) **28** (7), 2048 (1986) [Sov. Phys. Solid State **28**, 1145 (1986)].
4. H. H. Heikens, C. F. van Bruggen, and C. J. Haas, J. Phys. Chem. Solids **39** (8), 833 (1978).
5. H. H. Heikens, G. A. Wiegers, and C. F. van Bruggen, Solid State Commun. **24** (3), 205 (1977).
6. R. Tappero and A. Lichanot, Chem. Phys. **236** (1), 97 (1998).
7. Yu. A. Izyumov and Yu. N. Skryabin, Usp. Fiz. Nauk **171** (2), 121 (2001) [Phys. Usp. **44**, 109 (2001)].
8. Yu. A. Izyumov and B. M. Letfulov, in *Magnetism of Transition Metals and Alloys* (Yekaterinburg, 2000), pp. 42–60 [in Russian].
9. G. A. Petrakovskiĭ, S. S. Aplesnin, G. V. Loseva, L. I. Ryabinkina, and K. I. Yanushkevich, Fiz. Tverd. Tela (Leningrad) **33** (2), 406 (1991) [Sov. Phys. Solid State **33**, 333 (1991)].
10. B. Morosin, Phys. Rev. B **1** (1), 236 (1970).

Translated by G. Skrebtsov